ELSEVIER

Marine Chemistry 64 (1999) 7–27

MARINE CHEMISTRY

Sediment chronology in San Francisco Bay, California, defined by ^{210}Pb, ^{234}Th, ^{137}Cs, and ^{239,240}Pu

C.C. Fuller [a,*], A. van Geen [a,1], M. Baskaran [b], R. Anima [a]

[a] *Water Resources Division, U.S. Geological Survey, 345 Middlefield Rd., Menlo Park, CA 94025, USA*
[b] *College of Geoscience and Maritime Studies, Texas A&M University, Galveston, TX 77553-1675, USA*

Received 31 July 1997; revised 10 July 1998; accepted 17 July 1998

Abstract

Sediment chronologies based on radioisotope depth profiles were developed at two sites in the San Francisco Bay estuary to provide a framework for interpreting historical trends in organic compound and metal contaminant inputs. At Richardson Bay near the estuary mouth, sediments are highly mixed by biological and/or physical processes. Excess ^{234}Th penetration ranged from 2 to more than 10 cm at eight coring sites, yielding surface sediment mixing coefficients ranging from 12 to 170 cm^2/year. At the site chosen for contaminant analyses, excess ^{210}Pb activity was essentially constant over the upper 25 cm of the core with an exponential decrease below to the supported activity between 70 and 90 cm. Both ^{137}Cs and ^{239,240}Pu penetrated to 57-cm depth and have broad subsurface maxima between 33 and 41 cm. The best fit of the excess ^{210}Pb profile to a steady state sediment accumulation and mixing model yielded an accumulation rate of 0.825 g/cm^2/year (0.89 cm/year at sediment surface), surface mixing coefficient of 71 cm^2/year, and 33-cm mixed zone with a half-Gaussian depth dependence parameter of 9 cm. Simulations of ^{137}Cs and ^{239,240}Pu profiles using these parameters successfully predicted the maximum depth of penetration and the depth of maximum ^{137}Cs and ^{239,240}Pu activity. Profiles of successive 1-year hypothetical contaminant pulses were generated using this parameter set to determine the age distribution of sediments at any depth horizon. Because of mixing, sediment particles with a wide range of deposition dates occur at each depth. A sediment chronology was derived from this age distribution to assign the minimum age of deposition and a date of maximum deposition to a depth horizon. The minimum age of sediments in a given horizon is used to estimate the date of first appearance of a contaminant from its maximum depth of penetration. The date of maximum deposition is used to estimate the peak year of input for a contaminant from the depth interval with the highest concentration of that contaminant. Because of the extensive mixing, sediment-bound constituents are rapidly diluted with older material after deposition. In addition, contaminants persist in the mixed zone for many years after deposition. More than 75 years are required to bury 90% of a deposited contaminant below the mixed zone. Reconstructing contaminant inputs is limited to changes occurring on a 20-year time scale. In contrast, mixing is much lower relative to accumulation at a site in San Pablo Bay. Instead, periods of rapid deposition and/or erosion occurred as indicated by frequent sand-silt laminae in the X-radiograph. ^{137}Cs, ^{239,240}Pu, and excess ^{210}Pb activity all penetrated to about 120 cm. The distinct maxima in the fallout radionuclides at

* Corresponding author. Tel.: +1-650-329-4479; Fax: +1-650-329-4545; E-mail: ccfuller@usgs.gov
[1] Present address: Lamont-Doherty Earth Observatory, Palisades, NY, USA.

0304-4203/99/$ - see front matter © 1999 Elsevier Science B.V. All rights reserved.
PII: S0304-4203(98)00081-4

105–110 cm yielded overall linear sedimentation rates of 3.9 to 4.1 cm/year, which are comparable to a rate of 4.5 ± 1.5 cm/year derived from the excess ^{210}Pb profile. © 1999 Elsevier Science B.V. All rights reserved.

Keywords: sediment chronology; San Francisco Bay; radioisotope profiles

1. Introduction

Profiles of sediment-bound constituents such as metals and manmade organic compounds have been widely used to provide a record of contaminant inputs to lakes (Christensen and Goetz, 1987; Eisenreich et al., 1989), reservoirs (Callender and Robbins, 1994; van Metre et al., 1997) and estuarine and coastal environments (Santschi et al., 1984; Valette-Silver, 1993; Bopp et al., 1993; Krom et al., 1994; Ravichandran et al., 1995a). Such chronologies of contaminant inputs are dependent on the ability to establish the depositional history of the sediment column. For this purpose, sedimentation rates are commonly determined from profiles of radioisotopes such as ^{210}Pb (Appleby and Oldfield, 1992). However, physical and biological mixing processes can alter sediment radioisotope profiles. Quantifying sediment accumulation rates and the distribution of particle ages or deposition dates as a function of depth requires models that consider modification of profiles by mixing processes (Christensen and Bhunia, 1986; Robbins, 1987; Huh and Kadko, 1992). The time resolution for distinguishing changes in contaminant inputs is limited by the depth and rate of mixing (Robbins, 1987).

This paper presents sediment radionuclide profiles at two coring sites in the San Francisco Bay estuary: Richardson Bay near the estuary mouth and San Pablo Bay, about midpoint between the river delta and the ocean (Fig. 1). Chronologies for recent sediments (< 100 years) were derived from radionuclide profiles for evaluation of metal and organic contaminant profiles presented in subsequent papers in this series. At Richardson Bay, mixing coefficients for surface sediment were estimated from ^{234}Th/^{238}U disequilibria (Aller and Cochran, 1976). ^{234}Th (half-life 24.1 days) is produced by decay of dissolved ^{238}U in the water column and is strongly sorbed onto suspended sediment particles. The distribution of unsupported, or excess, ^{234}Th activity in sediments is indicative of sedimentation and mixing occurring within four months. Sediment accumulation rates were estimated from excess ^{210}Pb profiles (Appleby and Oldfield, 1992). Because of its 22.3 year half-life, ^{210}Pb provides indication of sedimentation occurring over the past 100 years. Sediment mixing and accumulation parameters were optimized by numerical simulation of ^{210}Pb profiles with a mixing/advection model. Profiles of atomic weapons testing fallout nuclides, ^{137}Cs and ^{239,240}Pu, were used for testing accumulation/mixing parameters at Richardson Bay and as time markers in San Pablo Bay because of their well-defined input history (Olsen et al., 1981; Callender and Robbins, 1994; Ravichandran et al., 1995b). These radionuclides first entered the environment about 1952. Maximum input occurred in 1963–1964 with 90% of fallout delivery between

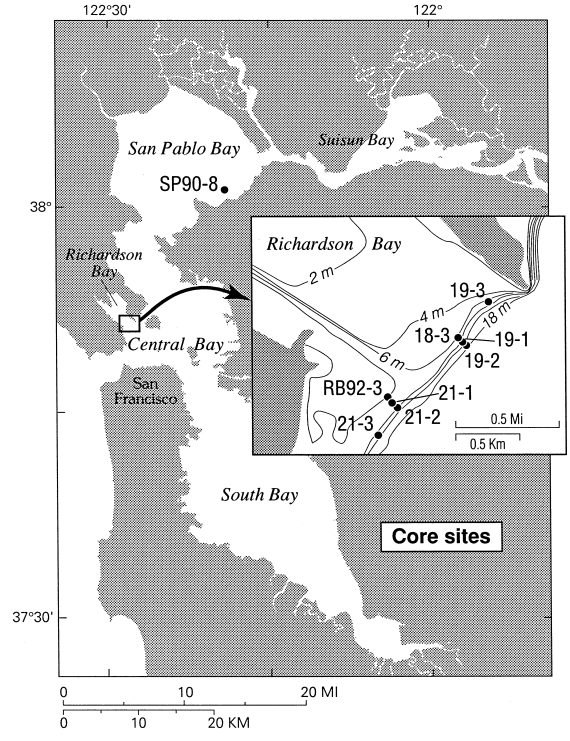

Fig. 1. Site map of coring sites. Inset for Richardson Bay shows bathymetry and location of box cores used for ^{234}Th.

1959 and 1964, and less than 3% after 1974 (Callender and Robbins, 1994).

1.1. Site description

Richardson Bay is a small embayment located 4.6 km northeast of the mouth of San Francisco Bay (Fig. 1). Tidal currents near the coring sites vary from 0.1 to 0.5 knots. Currents of up to 2.5 knots are observed in the main channel of the estuary outside the mouth of Richardson Bay. Cores were collected between 6 and 16 m of water near the top of a slope that drops to over 30 m in the main tidal channel outside the mouth of Richardson Bay (Fig. 1). The coring site in San Pablo Bay was located approximately 1.5 km from the axis of the main tidal channel in 4.5 m of water depth (Fig. 1). Currents at the location range from 0.5 to 2.9 knots. Seismic and bathymetry records indicate a slope of about 0.2% toward the main channel with the bottom being relatively flat.

2. Methods

2.1. Sample collection and processing

Eight stations at the mouth of Richardson Bay were occupied in August 1992. At each station one box core ($20 \times 30 \times 50$ cm deep), two 2-m gravity cores (9-cm inner diameter), and one 2-m rectangular freeze core (Crusius and Anderson, 1991) were collected within 9 m of each other. Stations were located along two transects parallel to the longitudinal axis of the bay along the depth gradient of the embayment mouth and at two additional sites (Fig. 1). The location of each core was determined by microwave navigation using shore based microwave transmitters.

Two 9-cm-diameter subcores were collected from each box core for radioisotope analysis. Subcores were sectioned by upward extrusion. Intervals from each pair of subcores were combined and homogenized. A subsample of each interval was dried to determine bulk density.

Gravity cores were kept vertical after recovery until sealed on ends. Gravity cores were stored at 4°C prior to X-radiography, density analysis by Gamma Ray Attenuating Porosity Evaluator (GRAPE) and magnetic susceptibility (Pereira et al., 1999). Cores were then split in half lengthwise, sealed and stored horizontally at 4°C. Sediment for radioisotope analyses (^{210}Pb, ^{137}Cs, ^{239,240}Pu) were subsampled at 2 to 3-cm depth intervals from the gravity core from site RB92-3 (Fig. 1) which was selected for contaminant analyses. Radioisotope subsamples were freeze dried. Samples of 1-cm width were subsampled at 10-cm intervals for grain-size analysis. Freeze cores were not used for analysis because irregular core tops indicated disturbance of the sediment surface.

A 2.3-m gravity core from San Pablo Bay (Fig. 1) was collected in 1990 using the same methods of collection and processing except that GRAPE measurements were not conducted. This site, SP90-8, was chosen because a weak acid extraction screening test suggested the core extended below apparent anthropogenic Zn inputs (Hornberger et al., 1999).

2.2. Radioisotope analyses

Total ^{234}Th activity was measured on intervals from the upper 10 cm of each box core from Richardson Bay by counting the 63 keV gamma emission with a high-resolution planar germanium detector spectrometer. Detector efficiency was determined by counting San Francisco Bay sediments previously analyzed for ^{238}U by isotope dilution alpha spectrometry following total decomposition and chemical separation (Fuller, 1982). The background corrected ^{234}Th count rate was corrected for self-absorption by measuring attenuation of a ^{234}Th source (1.4 g $UO_2(NO_3)_2 \cdot 6H_2O$ powder) placed on top of each sample container relative to an empty container (Cutshall et al., 1983). The supported activity of each core was defined by reanalyzing the deepest interval after five ^{234}Th half-lives had elapsed. Excess ^{234}Th activity, the difference between the initial count and the supported activity, was decay corrected for time elapsed between sample collection and counting. The reported uncertainty in the measured activities at the one standard deviation level was calculated from the random counting error of the peak and background regions (Friedlander et al.,

1981). Reported uncertainties do not include uncertainty in the detector efficiency.

Total ^{210}Pb activities were determined using isotope dilution of the ^{210}Po granddaughter and alpha spectrometry. About 2 g of freeze-dried sediment were digested in concentrated HCl, HF, and HNO_3 after the addition of a known activity of ^{208}Po or ^{209}Po as a yield monitor. Polonium from the solution was electroplated onto silver planchets (Flynn, 1968) and the isotopic ratio of ^{210}Po to the yield tracer planchet was assayed. The ^{208}Po and ^{209}Po yield tracers were calibrated with NIST traceable standards.

The supported ^{210}Pb activity, defined by ^{226}Ra, was determined on 5–10 g of freeze-dried sediment by gamma spectrometry at the 352 keV ^{214}Pb emission line (Baskaran and Naidu, 1995). Samples were counted on a high-purity Ge well detector that was calibrated with fly ash standards provided by the Environmental Measurements Laboratory.

Sediment ^{137}Cs activities were measured with the high-resolution intrinsic germanium, planar detector gamma spectrometer. The detector efficiency for ^{137}Cs was calibrated with two NBS Standard Reference materials (SRM 4350, 4350b). Gamma spectra were corrected for background and sample geometry (Hill et al., 1997). The reported uncertainty in the measured activity was calculated from the random counting error at the one standard deviation level. ^{137}Cs activities were corrected for radioactive decay between collection and counting.

^{239,240}Pu was determined by alpha spectrometry using the isotope dilution method. About 10 g of freeze-dried sediment was leached with hot 6 M HCl three times. The leachates were combined and a ^{242}Pu yield monitor was added. Pu was then separated from the leachate and purified using standard ion exchange techniques (Kressin, 1977; Ravichandran et al., 1995b). The purified Pu was electroplated onto stainless steel planchets and the ^{239,240}Pu activity was determined from the ratio of its alpha count rate to the ^{242}Pu tracer. The ^{242}Pu yield tracer was calibrated with NIST traceable standards.

Radioisotope inventories were calculated by integrating from the surface to deepest detectable measured activity with missing intervals linearly interpolated from adjacent measured intervals. Activities per gram were converted to activity per cm^2 by multiplying by the sediment bulk density for the mid-depth of each interval and by the interval thickness, then summed.

3. Results

3.1. Physical characteristics

The X-radiograph of core RB92-3 had few faint laminations. Either sediment mixing or deposition of a consistent sediment type has occurred throughout most of the 1.4-m length (Fig. 2). The core contains scattered shells below 50 cm and has relatively constant grain size in upper 60 cm (60% < 63 μm) with higher sand content below 60 cm (50%). The box cores from all eight sites all had abundant narrow (2–4 mm), cemented polychaete worm burrows at a density of about 5 to 10 burrows/9-cm diameter. Worm burrows extended to 12–15 cm where live organisms were present. Live burrowing shrimp (*Callianassa* sp.) were observed in gravity and freeze cores to depths of 30 cm or deeper at most Richardson Bay core sites. Shrimp burrows on order of 1–1.5 cm in diameter were visible in freeze-core slabs. The depth dependence of bulk density, ρ_z, (g dry sediment/cm^3 wet sediment) was calculated for core RB92-3 from a linear fit ($r = 0.8$) of the total density (determined by GRAPE, Pereira et al., 1999) vs. depth, z, to 120 cm, where $\rho_z = 0.00302z + 0.926$. A water density of 1.03 and particle dry density of 2.7 g/cm^3 were assumed.

In San Pablo Bay, distinct laminations were evident in the X-radiograph over the entire length of the core. Laminae of sandy sediment interbedded with silt layers were observed throughout the core (Fig. 2). Zones with high sand content ranged from a few mm to 5-cm thick. The numerous sand layers suggest that episodes of rapid deposition and/or scour have occurred. Sand layers occur most frequently between 110 to 170 cm. Few shell fragments were present. The absence of burrow structures and the presence of sand layers suggest that bioturbation probably is limited to silt layers prior to deposition of sand layers on top. The < 63 μm fraction (silt and clay) varies from 60 to 97% and is typically greater than

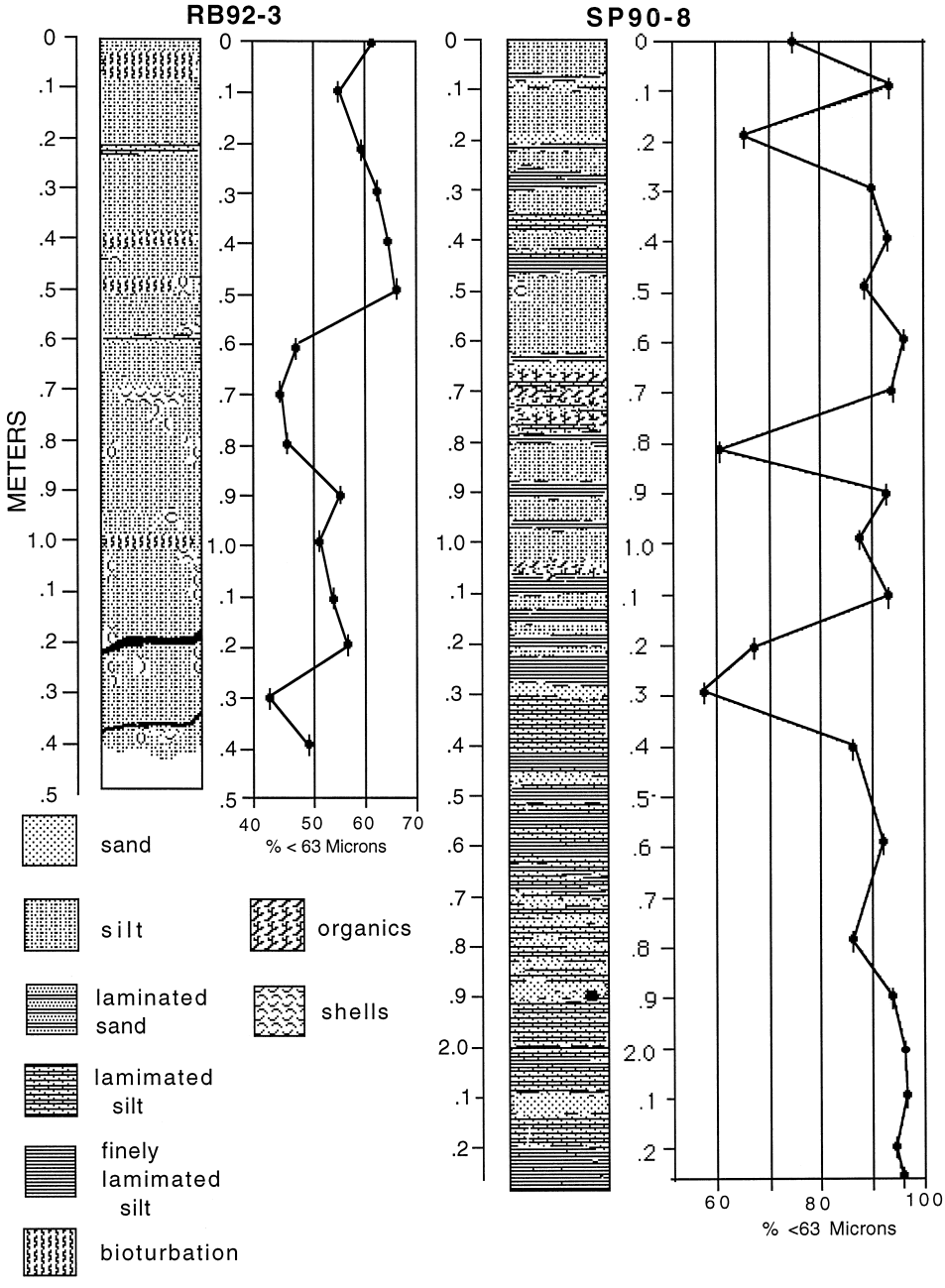

Fig. 2. Core descriptions from X-radiographs and visual observations and grain-size (% < 63 μm) vs. depth: (A) Richardson Bay gravity site RB92-3; and (B) San Pablo Bay site SP90-8. Grain-size measurements made on 1-cm-thick depth intervals, data points located on mid-depth of interval.

90% except at depths where sand layers and sand/silt laminae are present (Fig. 2). Sediments for radioisotope analyses were subsampled to avoid obvious sand laminae.

3.2. Radioisotope profiles

Excess ^{234}Th activity penetrated from 2 to > 10 cm and averaged 7 cm among the eight coring sites

in Richardson Bay (Table 1, Fig. 3). Excess ^{234}Th was observed to 5-cm depth at the core site chosen for contaminant measurement, RB92-3 (Fig. 3C). No trend was apparent between depth of excess ^{234}Th penetration and water depth of coring site.

At site RB92-3, total ^{210}Pb activity was nearly constant in the upper 25 cm (Fig. 4A) below which activity decreased to the supported activity represented by ^{226}Ra between 70 and 90 cm (Fig. 4A; Table 2). The activity and depth trends were comparable within the uncertainty of measured activity for the 35-cm box core and upper 35 cm of the gravity core. Little downcore variability was observed in ^{226}Ra, which averaged 1.06 ± 0.13 dpm/g. Excess ^{210}Pb (Fig. 4B) was calculated from the difference between the total ^{210}Pb and measured ^{226}Ra or the average ^{226}Ra for intervals not measured. The natural log of excess ^{210}Pb (Fig. 4C) decreased linearly from 20 to 30 cm to the bottom of the core.

Like ^{210}Pb, the box core and gravity core ^{137}Cs profiles are comparable. The activity profiles of ^{137}Cs and ^{239,240}Pu (Fig. 5A,B; Table 2) have broad subsurface maxima with highest activities between 33 and 41 cm. Both ^{137}Cs and ^{239,240}Pu activities decreased slightly towards the surface in the upper 30 cm of the sediment column. Both ^{137}Cs and ^{239,240}Pu were detected down to the 53 to 57-cm interval, below which measured activities were at or below the detection limit. The equivalent depth of maximum penetration of ^{137}Cs compared to strongly bound ^{239,240}Pu suggests little or no preferential, post-depositional mobility of ^{137}Cs.

Two zones of relatively uniform activity (Fig. 6A; Table 3) characterize the ^{226}Ra profile in San Pablo Bay. The upper 100 cm of sediment averaged 1.11 ± 0.21 dpm/g with significantly higher average activity of 1.53 ± 0.13 dpm/g measured between 120 and 170 cm. Below 170 cm, ^{226}Ra activity decreased but remained higher than the surface zone (1.37 ± 0.27 dpm/g). No significant correlation was found between ^{226}Ra and percent < 63 μm particles. The ^{226}Ra activity in the upper 100 cm is similar to the average from Richardson Bay.

Excess ^{210}Pb activity decreased about 30% between the surface and 100 cm, below which activity decreased rapidly to the supported activity by 120 cm (Fig. 6B). Excess ^{210}Pb activities in surface

Table 1
Richardson Bay box core ^{234}Th data: total activity represents decay corrected excess activity plus supported activity

Interval (cm) Top	Bottom	^{234}Th (dpm/g) total	$\pm\sigma 1$	^{234}Th(dpm/g) second count	$\pm\sigma 1$
Site RB92-3 box core					
0	2	3.85	1.26		
2	5	3.19	0.93		
5	10	1.88	0.24	1.88	0.15
Site RB18-3 box core					
0	2	9.98	1.06		
2	4	5.84	0.83		
4	6	4.11	0.49		
6	8	2.36	0.41		
8	10	1.94	0.25	1.73	0.12
Site RB19-1 box core					
0	2	5.07	0.96		
2	4	2.39	0.30		
4	6	2.27	0.34		
6	8	2.35	0.27		
8	10	2.64	0.28	2.29	0.18
Site RB19-2 box core					
0	2	7.52	0.84		
2	4	3.54	0.63		
4	6	1.75	0.60		
6	8	2.68	0.56		
8	10	1.71	0.25	1.72	0.11
Site RB19-3 box core					
0	2	3.18	0.69		
2	4	2.01	0.47		
4	6	2.64	0.94		
6	8	2.85	0.45	2.01	0.24
Site RB21-1 box core					
0	2	6.26	1.33		
2	5	4.03	1.21		
5	10	1.79	0.13	2.08	0.17
Site RB21-2 box core					
0	2	2.57	0.25		
2	5	4.02	0.42		
5	10	4.05	0.44	2.29	0.18
Site RB21-3 box core					
0	2	6.33	1.07		
2	5	6.26	1.17		
5	10	4.55	0.72	2.09	0.18

Second count is activity measured five or more half-lives after sample collection and equals the supported activity.
$\pm\sigma_1$ represents uncertainty of measured activity at one standard deviation level based on counting statistics.

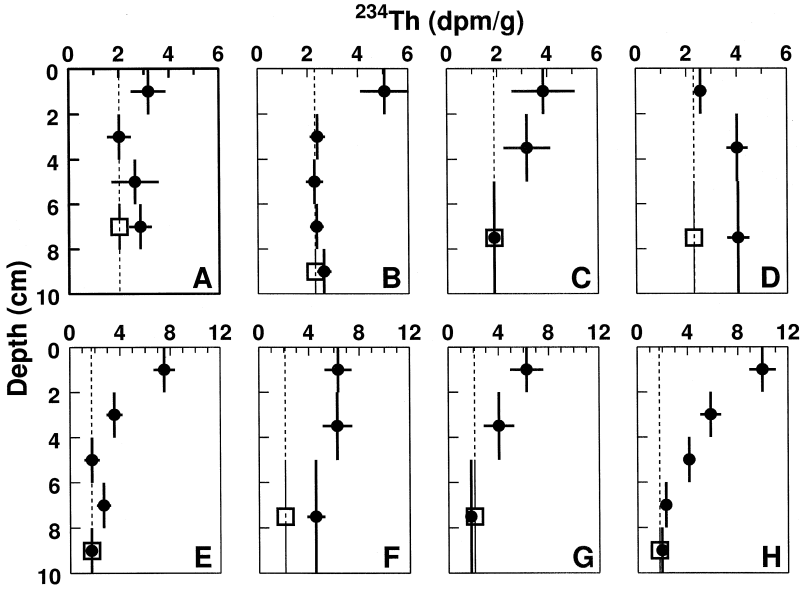

Fig. 3. ^{234}Th activity (dpm/g) vs. depth profiles from box cores from site (A) 19-3, (B) 19-1, (C) RB92-3, (D) 21-2, (E) 19-2, (F) 21-3, (G) 21-1, and (H) 18-3. Solid symbols represent total ^{234}Th with excess decay corrected to sampling date; open symbols represent supported activity determined from second count after five half-lives. Dashed line also represents supported activity. Vertical error bars indicate depth of sampling interval; horizontal error bars are the 1σ uncertainty in activity.

sediments were lower than observed in Richardson Bay. Below 113 cm, total ^{210}Pb activities were not significantly different than the activity supported by ^{226}Ra. A detection limit for measurable excess ^{210}Pb was estimated at 0.32 dpm/g for this core from two times the average σ_1 uncertainty in the difference

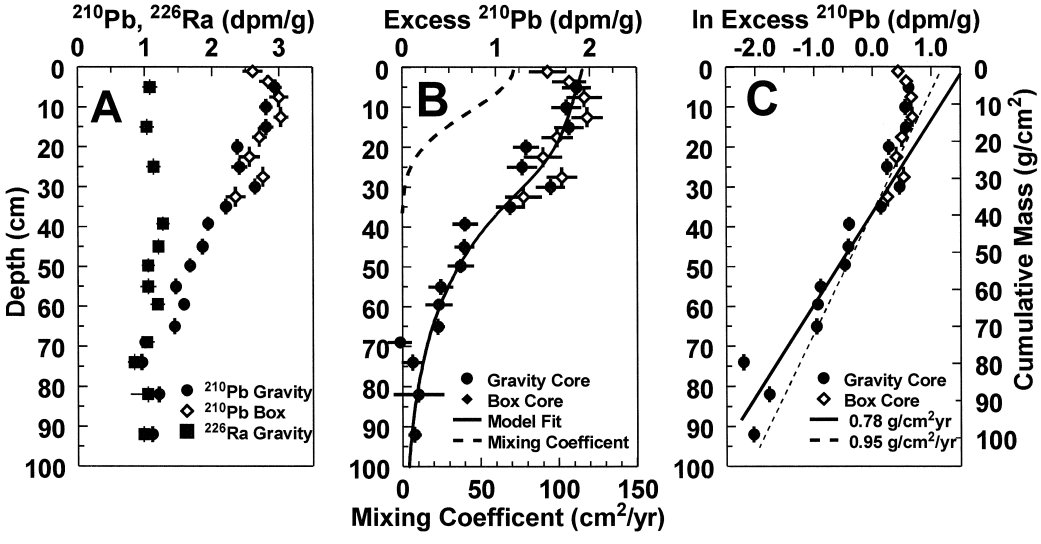

Fig. 4. Richardson Bay site RB92-3 radioisotope depth profiles: (A) total ^{210}Pb, ^{226}Ra activity (dpm/g) for box and gravity cores; (B) excess ^{210}Pb (dpm/g) with best-fit simulation of excess ^{210}Pb activity and mixing coefficient as function of depth; (C) ln excess ^{210}Pb vs. depth and cumulative solid mass with linear regression fits. Horizontal error bars in B represent the propagated 1σ uncertainty in excess ^{210}Pb from uncertainty in total ^{210}Pb and ^{226}Ra activities.

Table 2
Richardson Bay site RB92-3 ^{210}Pb, ^{226}Ra, ^{137}Cs, ^{239,240}Pu data: (A) box core; (B) gravity core

Interval (cm)		^{210}Pb (dpm/g)	$\pm\sigma 1$	^{226}Ra (dpm/g)	$\pm\sigma 1$	^{137}Cs (dpm/g)	$\pm\sigma 1$	^{239,240}Pu (dpm/g)	$\pm\sigma 1$
Top	Bottom								
A. Box core									
0	2	2.61	0.15			0.182	0.018		
2	5	2.84	0.13			0.233	0.022		
5	10	3.00	0.14			0.291	0.016		
10	15	3.03	0.11			0.309	0.024		
15	20	2.71	0.11			0.251	0.018		
20	25	2.56	0.16			0.271	0.018		
25	30	2.76	0.10			0.269	0.018		
30	35	2.35	0.15			0.302	0.020		
B. Gravity core									
3	7	2.94	0.11	1.08	0.11	0.300	0.047	12.4	1.9
8	12	2.81	0.10			0.206	0.027		
13	17	2.81	0.11	1.03	0.11	0.329	0.031	18.9	2.9
18	22	2.38	0.06			0.266	0.029		
23	27	2.41	0.12	1.13	0.11	0.253	0.033	18.7	2.3
28	32	2.64	0.09			0.309	0.033		
33	37	2.21	0.09			0.326	0.040	29.6	3.9
38	41	1.94	0.05	1.27	0.10	0.393	0.051	21.2	5.6
43	47	1.86	0.07	1.20	0.08	0.260	0.031	19.1	1.9
48	51					0.180	0.044	13.2	1.5
48	52	1.67	0.06	1.05	0.10				
53	57	1.46	0.06	1.05	0.12	0.124	0.064	5.3	0.9
58	61	1.58	0.07	1.19	0.11	0.007	0.047	1.4	0.3
63	67	1.44	0.07			0.029	0.027	1.2	0.7
68	70	1.00	0.03	1.03	0.11	0.024	0.036	0.9	0.6
72	76	0.95	0.07	0.84	0.10	0.009	0.018		
80	84	1.21	0.08	1.04	0.26				
84	87					0.002	0.029		
90	94	1.11	0.06	0.98	0.04				
94	97					0.000	0.027		

$\pm\sigma_1$ represents uncertainty of measured activity at one standard deviation level based on counting statistics. ^{210}Pb activity is decay corrected excess activity plus supported activity.

between measured ^{210}Pb and ^{226}Ra activities. The detection limit excess activity corresponds to an age of 60 years if the depositing sediment particles have an excess activity equal to the average excess ^{210}Pb activity of suspended sediments (2.0 ± 0.5 dpm/g, $n = 8$) measured in San Pablo Bay by Fuller (1982). All intervals below 115 cm in this core do not have measurable excess ^{210}Pb using this detection limit.

Both ^{137}Cs and ^{239,240}Pu activities increase by a factor of two from the surface to 90 cm and then increase rapidly to distinct maxima at 105 and 112 cm for ^{137}Cs and ^{239,240}Pu, respectively (Fig. 7; Table 3). The activity of both isotopes then decreases to below detection at the 120 to 123-cm interval. The near coincidence in activity maxima and in depths of maximum penetration argues against significant post-depositional mobility of ^{137}Cs.

4. Discussion

4.1. Surface mixing rates at Richardson Bay

Because of the ^{234}Th half-life (24.3 days), the presence of excess ^{234}Th at depth in sediment cores (Fig. 3) must result from rapid deposition or from post-depositional mixing of the sediment. Assuming the excess ^{234}Th profiles result from deposition alone, an apparent sediment accumulation rate can be calcu-

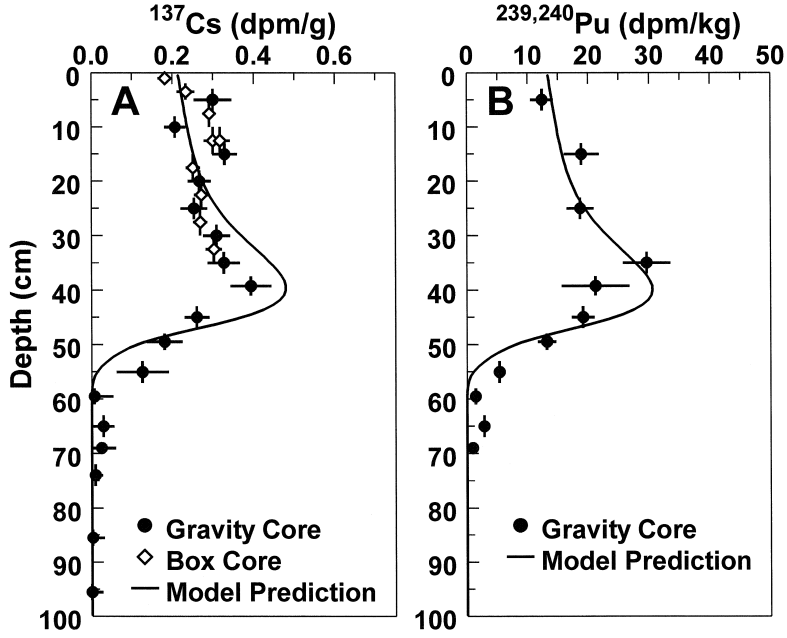

Fig. 5. Richardson Bay site RB92-3 radioisotope depth profiles: (A) ^{137}Cs (dpm/g); (B) ^{239,240}Pu (dpm/kg) for gravity and box cores. Vertical error bars indicate depth of sampling interval; horizontal error bars are the 1σ uncertainty in activity. Model simulated profiles were generated using the mixing and accumulation parameters optimized for ^{210}Pb and an incoming particle activity from the direct fallout record normalized to yield the observed ^{137}Cs or ^{239,240}Pu inventory.

lated by mass balance between the integrated excess ^{234}Th and the incoming particle activity as follows:

$$\rho_0 S_a C_o = \lambda_{Th} \int_0^z C_s \, \rho_z \, dz = \lambda_{Th} \phi_{Th}, \quad (1)$$

where, ρ_0 = sediment bulk density at surface, (g dry sediment/cm^3 of wet sediment); ρ_z = sediment bulk density at depth z; S_a = apparent linear sedimentation rate (cm/year); C_o = depositing particle excess ^{234}Th activity (dpm/g); λ_{Th} = ^{234}Th decay constant

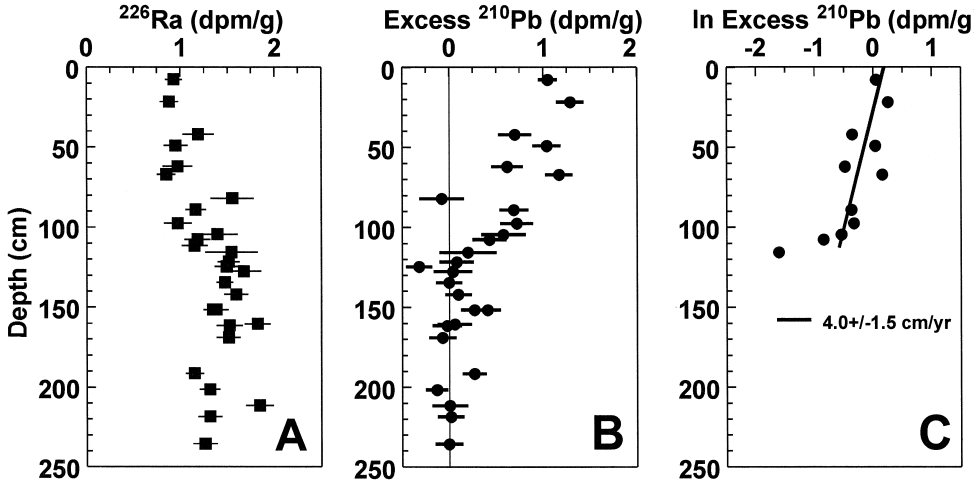

Fig. 6. San Pablo Bay site SP90-8 radioisotope depth profiles: (A) ^{226}Ra dpm/g vs. depth; (B) excess ^{210}Pb (dpm/g); ln excess ^{210}Pb with linear regression fit. Horizontal error bars in B represent propagated 1σ uncertainty in excess ^{210}Pb from uncertainty in total ^{210}Pb and ^{226}Ra activities.

Table 3
San Pablo Bay site SP90-8 ^{210}Pb, ^{226}Ra, ^{137}Cs, ^{239,240}Pu gravity core data

Interval (cm)		^{210}Pb (dpm/g)	$\pm\sigma 1$	^{226}Ra (dpm/g)	$\pm\sigma 1$	^{137}Cs (dpm/g)	$\pm\sigma 1$	$^{239,240}Pu$ (dpm/g)	$\pm\sigma 1$
Top	Bottom								
2	5					0.349	0.047		
6	9	1.98	0.05	0.93	0.09			6.3	1.2
10	13					0.369	0.033		
20	23	2.17	0.11	0.88	0.10	0.519	0.047		
30	33					0.471	0.036	2.9	0.5
41	43	1.89	0.06	1.19	0.17	0.426	0.058	9.2	1.2
46	48					0.528	0.038		
48	50	1.99	0.08	0.95	0.13	0.693	0.071		
61	63	1.59	0.06	0.97	0.16	0.340	0.044		
61	63					0.357	0.044	15.7	1.5
66	68	2.02	0.11	0.85	0.10	0.604	0.069		
70	73					0.382	0.033		
77	80					0.078	0.064		
81	83	1.47	0.06	1.55	0.23	0.602	0.047	10.5	1.6
87	89					0.639	0.044		
88	90	1.85	0.11	1.16	0.11	0.981	0.075		
96	99	1.90	0.09	0.97	0.15	0.755	0.060	19.9	1.4
99	103					1.192	0.075		
103	106	1.97	0.09	1.39	0.22	1.649	0.080		
106	109	1.61	0.12	1.18	0.14	1.057	0.067		
110	113			1.15	0.14	0.852	0.071	33.8	4.4
114	116					0.695	0.060	19.1	3.3
114	117	1.74	0.12	1.54	0.28				
117	119					0.289	0.051		
120	123	1.59	0.14	1.51	0.12	0.007	0.022	1.0	0.5
123	126	1.17	0.05	1.49	0.13	−0.062	0.038	0.3	0.1
126	129	1.71	0.08	1.67	0.19	0.013	0.038	0.1	0.1
133	136	1.47	0.11	1.47	0.09				
135	138					−0.016	0.038		
141	143	1.69	0.06	1.59	0.13	0.142	0.138		
150	153	1.75	0.10	1.34	0.10				
150	153	1.65	0.07	1.38	0.13	0.011	0.029	0.1	0.1
159	161	1.88	0.12	1.82	0.14				
160	163	1.50	0.07	1.52	0.14				
168	170	1.44	0.07	1.51	0.13				
190	193	1.42	0.08	1.15	0.1				
200	203	1.18	0.05	1.31	0.11				
210	213	1.85	0.12	1.84	0.15				
217	220	1.33	0.06	1.31	0.13				
234	237	1.26	0.07	1.26	0.13				

$\pm\sigma_1$ represents uncertainty of measured activity at one standard deviation level based on counting statistics. ^{210}Pb activity is decay corrected excess activity plus supported activity.

(per year); C_s = sediment excess ^{234}Th concentration (dpm/g); z = depth (cm); and ϕ_{Th} = integrated excess ^{234}Th (dpm/cm^2).

The average suspended sediment excess ^{234}Th activity, 27 ± 4 dpm/g ($n = 4$), measured near Richardson Bay (Fuller, 1982) was used for C_o, and agrees well with the average for nine sites throughout San Francisco Bay sampled in different seasons (24 ± 11 dpm/g, $n = 28$). S_a calculated from Eq. (1) ranges from 2 ± 0.4 to $> 32 \pm 5$ cm/year, averaging 12 ± 10 cm/year for the eight Richardson Bay sites, and 5 ± 1 cm/year at site RB92-3. Uncertainty

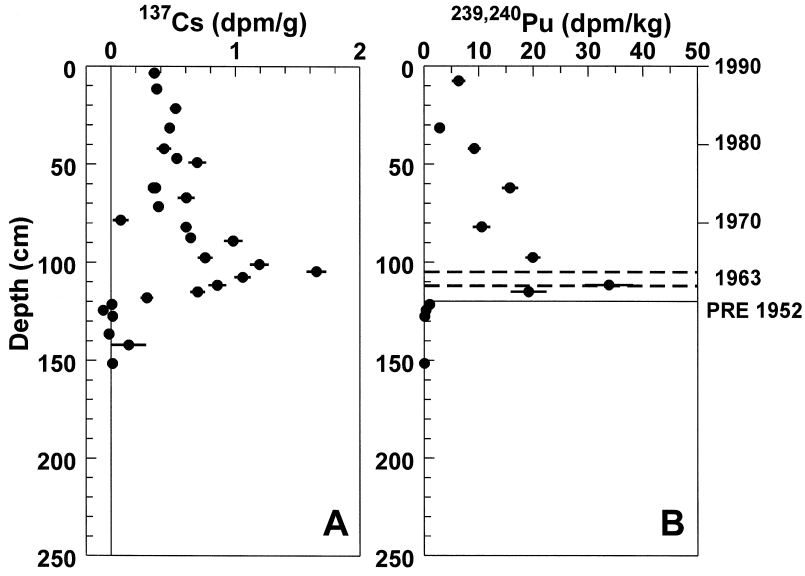

Fig. 7. San Pablo Bay site SP90-8 radioisotope depth profiles: (A) ^{137}Cs (dpm/g); (B) ^{239,240}Pu (dpm/kg). 1963 horizon fixed by maxima in fallout radionuclide activity; later dates assigned using constant linear sedimentation rate.

in S_a was propagated from the uncertainties in ^{234}Th count rates of sediment samples and from the uncertainty in the averaged value used for C_o. These rates are significantly higher than rates estimated from the other isotopes, to be shown later.

Assuming that the ^{234}Th profiles resulted instead from mixing, a one-dimensional sediment mixing coefficient, D_b, was calculated based on the model of Guinasso and Schink (1975) in which mixing was treated as a diffusional process:

$$D_b = S_a z, \tag{2}$$

where S_a equals the rate sediment particles are removed from the sediment water interface calculated using Eq. (1) and z is the maximum depth of excess ^{234}Th penetration. Mixing rate coefficients range from 12 ± 3 to 170 ± 35 cm^2/year and average 82 ± 54 cm^2/year for the eight sites. D_b of 25 ± 6 cm^2/year was calculated at site RB92-3.

Reworking of the sediments best explains the depth of ^{234}Th penetration in Richardson Bay. Biological and physical mixing of sediment column are the most likely causes, consistent with the presence of worm burrows penetrating to 12–15 cm in all cores and the presence of ghost shrimp at these sites. Because the measured ^{234}Th profiles reflect only conditions over the past 100 days at most, the variability of mixing depths and rates is unknown over the time scale of anthropogenic contaminant inputs (100 + years). However, the range of D_b estimated from the ^{234}Th profiles at all 8 sites provides an estimate of the possible long-term variability of mixing at Richardson Bay. The range of D_b is tested in numerical simulations of the ^{210}Pb profile for determining the long term mixing rate and depth at site RB92-3.

The calculated mixing coefficients are large compared to many other environments. For example, surface mixing coefficients have been reported ranging from 0.25 to 1 cm^2/year in the Hudson estuary (Olsen et al., 1981), 4 to 32 cm^2/year in New York Bight (Santschi et al., 1980), and up to 23 cm^2/year in Panama Basin (Aller and DeMaster, 1984). The surface D_b values calculated for Richardson Bay are comparable to other parts of San Francisco Bay and other estuaries. For example, Fuller (1982) observed ^{234}Th activity to depths of up to 15 cm with calculated D_b that ranged from 3 to 600 cm^2/year. In the Yangtze river estuary, mixing rate coefficients ranging from 20 to 260 cm^2/year were calculated from

excess ^{234}Th profiles that penetrated to 12 cm (McKee et al., 1984).

4.2. Sedimentation rates

Steady state sediment accumulation rates were estimated from the slope of the linear regression of the ln ^{210}Pb excess activity vs. depth using the constant flux-constant sedimentation rate model (Appleby and Oldfield, 1992). This model assumes a steady state accumulation of sediments and that the excess ^{210}Pb activity of depositing sediment particles is constant. To account for compaction at site RB92-3, linear regression of the ln excess ^{210}Pb (dpm/g dry sediment) vs. the cumulative dry mass (g/cm^2) calculated from the bulk density vs. depth was used to estimate the sediment accumulation rate, ω, in units of g/cm^2/year. The regressions were truncated below the 63 to 67-cm interval because of the large relative uncertainty of the excess ^{210}Pb activities below this depth. Varying the shallowest depth used in the regression from 25 to 12 cm resulted in sediment accumulation rate that increased from 0.78 $\pm$ 0.08 to 0.95 $\pm$ 0.08 g/cm^2/year. The 0.78 g/cm^2/year rate (25–67 cm) had the highest regression correlation coefficient ($r = 0.96$) and is shown in Fig. 4C along with the second best fit of 0.95 g/cm^2/year (12–67 cm, $r = 0.94$) for comparison. These rates are equivalent to surface linear sedimentation rates of 0.84 and 1.0 cm/year, respectively, and average rates for the upper 100 cm of 0.72 and 0.88 cm/year using the average density over that depth range.

Sediment accumulation rate, ω, also was estimated independently of sediment mixing by mass balance between the integrated excess ^{210}Pb activity with the incoming particle activity, where ω equals $S_a \rho_0$ in Eq. (1). This method is independent of profile shape or depth of excess ^{210}Pb penetration. At Richardson Bay, ω of 0.49 $\pm$ 0.25, 0.61 $\pm$ 0.02, and 0.83 $\pm$ 0.06 g/cm^2/year are calculated using suspended sediment activities (Fuller, 1982) equal to the average for the Golden Gate (4.6 $\pm$ 2.3 dpm/g, $n = 4$), the riverine endmember (3.7 $\pm$ 0.1 dpm/g, $n = 4$), and the bay wide annual average (2.7 $\pm$ 0.2 dpm/g, $n = 39$), respectively, for C_o. Although the mass balance derived rates are dependent on C_o, which is not well constrained at this site, these rates are similar to or lower than the best fit rate from the ln excess ^{210}Pb vs. cumulative mass of 0.78 $\pm$ 0.08 g/cm^2/year. The range of sediment accumulation rates from both methods was tested later in numerical model simulations of ^{210}Pb profiles to optimize the accumulation rate and mixing rate.

The broad subsurface maxima and the persistence of ^{137}Cs and ^{239,240}Pu in the upper 20 cm could be caused by post-depositional mixing of the sediment column, by continued input from erosion in the drainage basin (Olsen et al., 1981; Callender and Robbins, 1994), and/or by redistribution of sediments within the estuary through cycles of resuspension, transport and deposition. Assigning a date of 1952 to 57 cm, the maximum depth of penetration, an overall sedimentation rate of 1.4 cm/year was inferred, that is significantly greater than estimates from ^{210}Pb. This contrast indicates either a higher sedimentation rate during part or all of the last 40 years, or that the sediment mixing has increased the depth of penetration. The latter is consistent with the presence of burrowing organisms and with the excess ^{210}Pb and ^{234}Th profiles. Assuming the upper 25 cm is rapidly mixed, based on the nearly constant excess ^{210}Pb, a sedimentation rate of about 0.8 cm/year is estimated from the maximum depth of fallout nuclide penetration.

In San Pablo Bay, an overall linear sedimentation rate of 4.5 $\pm$ 1.5 cm/year is calculated from the slope of linear regression between of ln excess ^{210}Pb and depth to 109 cm ($r = 0.7$, Fig. 6C). This overall rate includes sand layers, which probably result from episodic events of rapid deposition and/or scour. The mass balance method to estimate accumulation rate can not be applied to the San Pablo Bay core because the profile is not complete (see below). Overall sedimentation rates of 3.9 and 4.1 cm/year are calculated by assigning a date of 1963 to the ^{137}Cs and ^{239,240}Pu activity maxima at 105 and 112 cm. These rates are within the uncertainty of the ^{210}Pb derived rate. These rates also are significantly higher than determined from ^{210}Pb and ^{137}Cs in earlier studies in this part of the estuary, 1.3 cm/year (Fuller, 1982). The distinct maxima in both ^{137}Cs and ^{239,240}Pu and the frequent sand laminae are consistent with significantly less mixing compared to Richardson Bay. Because of less mixing, the presence of

^{137}Cs and ^{239,240}Pu in surface sediments suggests continued input both from redistribution of sediment within the estuary and from erosion in the drainage basin.

4.3. Sediment focusing

Sediment focusing or trapping efficiency for a site can be estimated from the focusing factor, FF, which is the ratio of the measured radioisotope inventory, ϕ, to the inventory expected due to direct input (Aller et al., 1980; Wong et al., 1995). FF includes focusing of radioisotopes both from the drainage basin and from within the estuary. An FF of one or more is indicative of net accumulation of sediment. The direct input of excess ^{210}Pb is defined as the activity supported by direct ^{210}Pb atmospheric fallout to the San Francisco Bay area (Fuller and Hammond, 1983). Direct inputs of ^{137}Cs and ^{239,240}Pu were calculated from the monthly atmospheric flux of ^{90}Sr measured from 1952 to 1976 at Richmond, CA (Health and Safety Laboratory, 1976), about 10 km from Richardson Bay, times fission production yields of 1.65 and 0.017 for ^{137}Cs and ^{239,240}Pu relative to ^{90}Sr (Simpson et al., 1980; Callender and Robbins, 1994). Monthly ^{137}Cs fallout was decay corrected to the coring date. The direct input source of excess ^{234}Th was defined as the decay of dissolved ^{238}U integrated over the water depth at each coring location. A constant ^{238}U concentration of 2.2 dpm/l (Fuller, 1982) was used based on the average salinity of 31 ± 1‰ for the four months prior to core collection (Schwartz, 1998).

At Richardson Bay, ^{210}Pb, ^{137}Cs, and ^{239,240}Pu focusing factors of 15, 3.5 and 12 at site RB92-3 were calculated from ϕ_{Pb} of 72.5 dpm/cm^2, ϕ_{Cs}, of 16.0 dpm/cm^2, and ϕ_{Pu} of 1.02 dpm/cm^2, respectively. The FF for all radioisotopes indicated a high degree of sediment focusing and, therefore, net accumulation. The much lower FF for ^{37}Cs compared to ^{210}Pb or ^{239,240}Pu could be due to either loss of ^{137}Cs by desorption from sediments prior to deposition at this site (Olsen et al., 1993) or to its lower affinity to particle surfaces. FF estimated from ^{234}Th ranged from 2 to > 13, averaged 7 ± 5 for the eight coring sites, with a value of 5 at site RB92-3. The ^{234}Th input term does not account for the range of water depths and variations in salinity and suspended sediment concentration particles encounter before deposition. The ^{234}Th focusing factors, therefore, have a greater uncertainty than the FF derived from ^{210}Pb and ^{239,240}Pu, which may account for the lower values. In addition, ^{234}Th focusing factors are indicative of conditions during the last 100 days. Nonetheless, the greater than one ^{234}Th focusing factors are consistent with net accumulation at this site.

At San Pablo Bay, integrated ^{137}Cs and ^{239,240}Pu activities of 73 dpm/cm^2 and 1.6 dpm/cm^2 were estimated assuming a constant bulk density of 1.1 g/cm^2, the ρ_z at 60 cm in core RB92-3. These values of ϕ_{Cs} and ϕ_{Pu} yield focusing factors of 15 and 19, respectively. The closer agreement between the ^{137}Cs and ^{239,240}Pu derived focusing factors at San Pablo Bay compared to Richardson Bay suggests that significant ^{137}Cs was lost from sediments prior to deposition at Richardson Bay. Sediment focusing factor was not calculated from ^{210}Pb because the profile may not be complete as a result of an inferred erosional period (discussed below).

4.4. Numerical simulation of radioisotope profiles

The lack of laminated sediments, the presence of burrowing organisms, the depth of excess ^{234}Th activity, the constant excess ^{210}Pb activity in the upper 25 cm, and the depth of penetration and shape of the bomb fallout nuclide profiles all are consistent with rapid and deep mixing of the sediments at site RB92-3 in Richardson Bay. Sediment accumulation rates in mixed sediments are typically estimated by fitting measured radioisotope profiles to an advection/diffusion model (Robbins and Edgington, 1976; Turekian and Cochran, 1978; Huh and Kadko, 1992). For Richardson Bay, numerical simulation was used to determine the sedimentation and mixing parameters that best fit the observed ^{210}Pb profile. Then ^{137}Cs, ^{239,240}Pu and hypothetical contaminant profiles were simulated using the accumulation and mixing parameter sets that produced the best fit to the ^{210}Pb profile. A sediment chronology was developed from profiles of simulated hypothetical contaminant inputs. The San Pablo Bay profiles were not simulated because the frequent sand laminae indicate mixing was limited to silt layers prior to sand deposition and was therefore not a continuous process.

4.5. Numerical sedimentation-mixing model

Profiles were simulated by solving by finite difference the diagenetic equation for radionuclide concentration (Appleby and Oldfield, 1992):

$$\frac{\mathrm{d}\rho C}{\mathrm{d}t} = \frac{\partial}{\partial z}\left(D_{\mathrm{b}}\frac{\partial \rho C}{\partial z}\right) - \frac{\partial S\rho C}{\partial z} - \lambda\rho C, \qquad (3)$$

where C = concentration at any depth z (atoms/g); ρ = sediment density at depth z (g dry sediment/cm^3); S = linear sedimentation rate (cm/year); λ = decay constant (per year); and D_{b} = mixing coefficient at depth z (cm^2/year).

Sediment mixing was treated as a diffusive process based on the model of Goldberg and Koide (1962) in which the sediment column consists of a mixed zone underlain by a zone with no mixing. Exponential and half-Gaussian functions were used for the depth dependence of D_{b}. An exponential decrease in D_{b} from the sediment surface, EXP (Olsen et al., 1981) or from below a zone of constant mixing, MZ/EXP (Peng et al., 1979) was defined as:

$$D_{\mathrm{b}}(z) = D_{\mathrm{b}}(o)\, e^{-\left(\frac{0.693Z}{H}\right)}, \qquad (4)$$

where H equals depth at which $D_{\mathrm{b}}(z)$ equals 0.5 times $D_{\mathrm{b}}(o)$ of the surface or constant mixed zone. The half-Gaussian depth dependence of D_{b} also was tested of the form:

$$D_{\mathrm{b}}(z) = D_{\mathrm{b}}(o)\, e^{-\left(\frac{z^2}{2\gamma 2}\right)}, \qquad (5)$$

where γ is the mixing depth parameter. Christensen and Bhunia (1986) found that the half-Gaussian depth dependence of D_{b} yielded better fits to ^{210}Pb and ^{137}Cs profiles than the exponential depth dependence of D_{b}. Eq. (5) was used to calculate D_{b} both from the sediment surface, HG, and from below a zone of constant mixing rate, MZ/HG. The MZ/EXP and MZ/HG submodels have four parameters: sedimentation rate, S, surface mixing coefficient, $D_{\mathrm{b}}(o)$, constant mixed zone depth, MZ, and the $D_{\mathrm{b}}(z)$ parameter, H or γ. The EXP and HG submodels have three variable parameters, S, $D_{\mathrm{b}}(o)$, and H or γ.

Eq. (3) was solved by iterating over finite time intervals (Peng et al., 1979 and Olsen et al., 1981). The simulations assumed steady state conditions for sedimentation, mixing, and incoming particle ^{210}Pb activity. The model operates as outlined by Olsen et al. (1981) modified to account for compaction by initially dividing the sediment column into layers of equal mass based on the depth dependence of bulk density starting with a 1-cm surface layer. When the total mass of the surface layer has increased by a factor of two from accumulation, sediment is advected downward by dividing the surface layer into two parts of equal activity. The thickness of each layer is determined by ρ for its new depth. The initial concentration was set to the supported activity for ^{210}Pb, or zero for fallout radionuclides and hypothetical contaminants. The sediment mass accumulation rate, ω, is used in the model to calculate the linear sedimentation rate for each layer by dividing by ρ. To minimize numerical dispersion and overflow, the model layer thickness and time step duration were set so that the mean particle diffusion distance over one time step was less than 10% of the layer thickness for the highest $D_{\mathrm{b}}(o)$ used (170 cm^2/year).

A goodness of fit parameter, χ^2, was determined for each simulation, as follows:

$$\chi^2 = \Sigma\frac{(C_{\mathrm{m}} - C_{\mathrm{f}})^2}{C_{\mathrm{m}}}, \qquad (6)$$

where C_{f} is fit concentration and C_{m} is the measured concentration. The smaller the χ^2 value, the better the fit overall to the data set. The χ^2 values are unique to the specific constituent simulated (e.g., ^{210}Pb, ^{137}Cs).

4.6. ^{210}Pb simulations

^{210}Pb simulations were run for two hundred years to obtain steady state activity profiles. Instead of optimizing all parameters simultaneously, the parameters were varied systematically starting with the range of sediment accumulation and surface mixing coefficients estimated from core data for ^{210}Pb at RB92-3 and from ^{234}Th at the eight box core sites. The four submodels of depth dependence of mixing rate were tested over a range of mixing depths. The depositing particle excess ^{210}Pb activity, C_{o}, used in each simulation was fixed by mass balance (Eq. (1)) between the measured integrated excess ^{210}Pb, ϕ_{Pb},

and the specific sediment accumulation rate used in that simulation. The ϕ_{Pb} of model generated profiles were within 1% of the measured ϕ_{Pb}.

χ^2 values ranged from 0.390 for the best fit to 4.48 for a simulation with no mixing. For comparison, a χ^2 of 0.470 was calculated for the measured excess ^{210}Pb and 1 sigma, σ_1, measurement uncertainty for each subsample, where $C_f = C_m + \sigma_1$ in Eq. (6). ^{210}Pb fits that were within the uncertainty of measured data ($\chi^2 < 0.470$) were obtained only with the HG and EXP submodels. The best fit (χ^2 0.390) was found for sediment accumulation rate of 0.825 g/cm^2/year, surface mixing coefficient of 71 cm^2/year, and a half-Gaussian mixing rate depth dependence of 9. The base of the mixed zone is defined as 33 cm where $D_b(z)$ is less than 0.1% of surface D_b (Fig. 4B). This accumulation rate is within the uncertainty of ω derived from linear regression of the ln excess ^{210}Pb, 0.78 ± 0.08 g/cm^2/year. The value of D_b averaged over the upper 10 cm, 63 cm^2/year, agrees well with the average D_b, 82 cm^2/year, determined from eight ^{234}Th profiles but is about 2.5 times D_b determined from the ^{234}Th profile at site RB92-3. D_b derived from numerical simulation represents the average mixing rate for the last 100 years, while D_b estimated from the ^{234}Th profile only represents conditions over about 100 days prior to coring. This difference in mixing rate may result from temporal changes in population density and activity of burrowing organisms and/or variability in processes causing physical mixing.

4.7. ^{137}Cs *and* ^{239,240}Pu *simulations*

^{137}Cs and ^{239,240}Pu profiles were simulated with the parameter values that yield the best fit to the ^{210}Pb profile. The measured annual fallout between 1952 and 1976 (Health and Safety Laboratory, 1976) scaled to yield the measured integrated activity was used for the input function. Additional fallout inputs that result from soil erosion in the watershed and from redistribution of sediments within estuary, which likely lag behind direct atmospheric deposition flux (Olsen et al., 1981; Callender and Robbins, 1994) are not known. Because the time dependence of these inputs is not known, the ^{137}Cs and ^{239,240}Pu profiles simulated from the scaled direct fallout input function only can be used to compare the maximum depth of penetration and the peak in measured profiles.

The ^{137}Cs simulation (Fig. 5A) had a χ^2 of 0.163, compared to a χ^2 of 0.099 calculated from the measured ^{137}Cs and 1 sigma, σ_1, measurement uncertainty for each subsample, where $C_f = C_m + \sigma_1$ in Eq. (6). The ^{239,240}Pu simulation (Fig. 5B) yielded a χ^2 of 4.91 compared to χ^2 of 3.89 calculated from the measured ^{239,240}Pu and its σ_1. The model accurately predicted the maximum depth of penetration but underestimated the activity of the deepest interval. The depth of the simulated profile maximum at 39 cm agrees well with the observed ^{137}Cs peak at 39–41 cm, but is slightly deeper than the ^{239,240}Pu peak at 33–37 cm. The ^{239,240}Pu peak is not as well defined as the ^{137}Cs peak. The peak activity is over estimated for both isotopes and the activity between the peak and the sediment surface is under predicted for ^{137}Cs. These differences are likely due to not including the time dependence of watershed and internal redistribution components in the model input function. The agreement between simulated and observed ^{137}Cs and ^{239,240}Pu profiles suggest that the steady state accumulation and mixing parameters derived from ^{210}Pb profile provide an adequate description of conditions at this site.

Because ^{137}Cs sediment profiles also are affected by post-depositional desorption and diffusional transport, the ability of a mixing-accumulation model to simulate a ^{137}Cs profile is not evidence itself for the dominance of mixing on controlling profile shape (Smith and Comans, 1996). However, because Pu is significantly less mobile in porewaters (Crusius and Anderson, 1995), the similar maximum penetration depth for ^{239,240}Pu and ^{137}Cs combined with the model predictions argues for the dominance of mixing over remobilization in development of the ^{137}Cs profile observed at this site.

4.8. *Apparent sediment chronology at Richardson Bay*

4.8.1. *Effect of mixing on contaminant profiles*

The sediment accumulation and mixing parameters optimized by fitting the ^{210}Pb profile (ω, 0.825 g/cm^2/year; $D_b(o)$, 71 cm^2/year; γ, 9 cm) were used to simulate successive 1-year duration pulse

inputs of a hypothetical nonreactive contaminant of 100 units/cm^2. The profiles were allowed to evolve in 1-year increments to 140 years after deposition of the pulse. Fig. 8 shows profiles for each of five depositional years illustrating the effect of the high degree of mixing. The age distribution of particles at each depth and a chronology for interpreting contaminant profiles are determined from these simulations.

Because the pulse input was set to yield a total integrated concentration of 100 units/cm^2, the concentration per cm^2 at any depth horizon equals the percent of that year's total input. After deposition, each 1-year pulse is diluted over time by mixing with both older sediments and subsequently deposited material. A peak in concentration develops as the pulse is advected downward; the peak decreases in concentration over the first 20 years after deposition. The peak is eventually buried below the mixed zone where its concentration remains constant and is retained in the sedimentary record. Even after the contaminant peak has been advected through the mixed zone, a fraction of the contaminant remains in the mixed zone and undergoes continued dilution by mixing with subsequently deposited sediments (Fig. 8). Comparison of the integrated contaminant concentration in the mixed zone to the total amount deposited indicates that more than 95% of a contaminant remains within the mixed zone 12 years after deposition of a 1-year pulse input. After 20 years, about 82% remains, 50% after 33 years, and 25% after 50 years. Over 75 years are required to bury 90% of contaminant below the mixed zone. The fraction of a contaminant remaining in the mixed zone from a single year's input decreases exponentially after the peak concentration has been advected through the mixed zone (20 years). A first-order fit indicates that the fraction of contaminant remaining in the mixed zone decreases with a half-life of 18 years after the peak has been buried below the mixed zone.

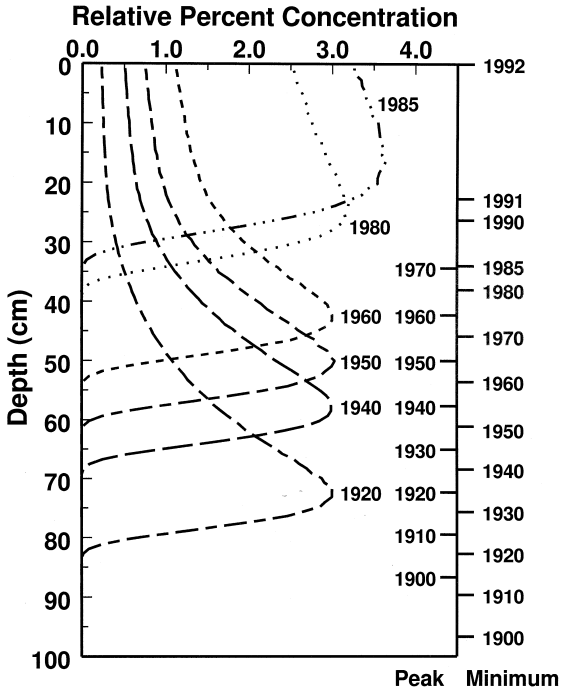

Fig. 8. Simulated depth profiles in 1992 for five deposition periods of 1-year inputs of a hypothetical nonreactive contaminant. Profiles were simulated using the mixing and accumulation parameters were derived from ^{210}Pb. Year of deposition is shown for each profile. Relative concentration is plotted as the percent of 1-year pulse vs. depth. The date scales on the right correspond to (1) the most recent date of deposition for sediment particles comprising a depth horizon, denoted as minimum age, and (2) the year of input for the sediment particles that have the greatest mass abundance at that depth, denoted as peak. These dates were determined from the age distribution of sediments as a function of depth (see text).

The fractional mass contribution of sediment from a year to a depth interval was determined by dividing the concentration per cm^2 for that year by the sum of contaminant concentration for all years. Plotting the mass contribution of each year at representative depths illustrates the wide age distribution of particles in each horizon (Fig. 9). For example, the 50-cm horizon is composed of sediments deposited as recently as 1965 to before 1850, with 1950 having the greatest mass abundance.

4.8.2. Age model for interpreting contaminant profiles

A unique date or age cannot be assigned to any depth horizon because sediment particles with a wide range of deposition dates occur at each depth. However, a chronology can be developed by assigning the minimum age of deposition and a date of peak deposition to each depth. The minimum age, shown at 10-year increments in Fig. 8, is defined as the most recent date of deposition of sediment particles in a depth horizon (Fig. 9). At the deepest depth a contaminant is detected, the minimum age corre-

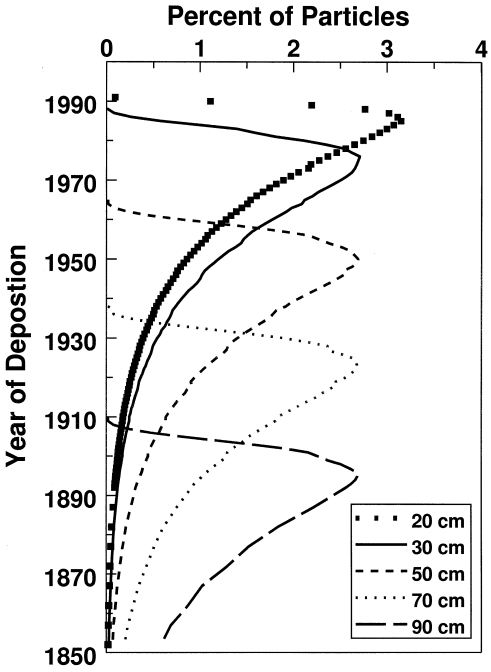

Fig. 9. Age distribution of sediment particles at five depths plotted as the percent of sediment mass in each horizon vs. year of deposition. Age distribution was derived from profiles of 1-year pulse contaminant input simulated for 1 to 140 years after contaminant deposition.

sponds to the date that contaminant was first deposited. Because of the high degree of mixing, sediments deposited within the last year are distributed over the upper 25 cm. Therefore the most recent date of deposition for upper 25 cm is within the last year. The date of peak concentration is defined as the year of deposition with the greatest mass abundance for that depth (Fig. 9). The peak year of input (Fig. 8) for a contaminant corresponds to the depth interval with the highest concentration of that contaminant.

Interpreting contaminant profiles at this site is thus limited to estimating the date of first appearance of particle bound contaminants from its maximum depth of penetration and to estimating the peak year of input if a concentration maximum occurs in the profile. For example, the chronology model suggests that the age of first appearance at 59 cm is 40 years or a date of 1952 (Fig. 8). This date corresponds to the onset of significant fallout of radionuclides from nuclear weapons testing and agrees well with the observed maximum depth of penetration of detectable ^{137}Cs and ^{239,240}Pu, 57 cm. Contaminant inputs are unlikely to be deposited in uniform 1-year pulses. Inputs of longer duration would result in broader peaks with the concentration maximum corresponding to the midpoint in time of input provided that the input function is either uniform or symmetrical, or is dominated by a specific period. For example, the maximum fallout radionuclide input in 1963 corresponds to a depth of 39 cm, which agrees well with maximum ^{137}Cs activity observed in the 39 to 41-cm interval.

The chronology for site RB92-3 described above assumed that the net sedimentation rate and mixing regime are relatively constant over the past 140 years. However, a relatively rapid transition appears to occur around the turn of the century. A sedimentation rate of 0.07 cm/year was inferred from ^{14}C ages of individual shell fragments found at 110 and 140 cm (van Geen et al., 1999). An increase in ^{10}Be between 77 and 85 cm and the presence of fossil fuel biomarkers at 80 cm (Pereira et al., 1999) are the earliest evidence of human activity recorded in this core. The ^{10}Be increase is presumed to result from accelerated erosion during development of the watershed (van Geen et al., 1999). Because no other data are available to better constrain the onset of this apparent change in accumulation rate or to determine the rate of change, the chronology below 80 cm (Fig. 8) is an extrapolation into this uncertain transition period.

Some important implications stem from the rapid and deep reworking of sediments by biological and/or physical processes at RB92-3. A contaminant is diluted rapidly to 10% of the depositing particle concentration in the surface 1-cm after 1 year. As a result, the sediment concentration at the time of deposition could have been significantly higher than observed in buried horizons, especially if deposition occurred over a short period of time. Contaminants will persist in the mixed zone sediments for many years after deposition. After 33 years, 50% of a contaminant still remains in the mixed zone with the concentration diluted to 1% of the initial concentration.

4.8.3. Reconstructing contaminant fluxes

Reconstructing historical changes in contaminant inputs is valuable in understanding the fate of con-

taminants in the estuary, but the ability to discern changes in a contaminant input or flux is limited by the rate and depth of mixing. Intrinsic resolution is defined as the minimum time required between two pulse event inputs to result in two discernible maxima in a contaminant profile (Robbins, 1987). Resolution is quantified as the number of years between pulses required to yield a concentration minimum between peaks equal to 50% of the average peak concentration (Robbins, 1987). A 32-year separation between two simulated pulse inputs was required to meet this criterion at Richardson Bay. Pulses occurring at intervals of less than 15 years would result in a single maximum. At 20-year separation, a second, deeper peak appears as a shoulder to the shallower peak.

Christensen and Goetz (1987) proposed a method to deconvolute sediment profiles for reconstructing contaminant fluxes to the sediment surface as a function of time. Briefly, the flux of a contaminant is determined from the concentration profile as follows:

$$C_z = \sum_{j=1}^{n} \mathbf{F}_{zj} J_{n+1-j} \qquad z = 1,2,3,\ldots,n, \tag{7}$$

where z and j are depth and time intervals, C_z is the concentration depth profile, **F** is a matrix of fractional contribution of particles to each depth interval for a given time interval, and J is the flux of contaminant to the sediment. Matrix **F** is generated by summing the fractional contribution to each depth interval by year from the simulation (Eqs. (3) and (5), Fig. 9) of 1-year pulses. **F** is inverted and multiplied by the measured concentration profile to determine J. The time and depth intervals over which fluxes can be successfully calculated are dependent on the degree of mixing.

The deconvolution model was tested for site RB92-3 with hypothetical contaminant profiles generated from multiple pulse and stepped inputs using the forward simulation model. Time intervals of less than 20 years or depth intervals smaller than 15 cm for **F** did not successfully reconstruct these known inputs. However, fluxes were reproduced to within 10% for each 20-year interval with best results obtained for a 33-cm surface zone underlain by 15-cm intervals. The results of this exercise suggest that changes in the input function of a contaminant of less than 20 years can not be extracted from the sedimentary record at this site. The 20-year interval for reconstructing contaminant fluxes is significantly better than the calculated 32-year intrinsic resolution, but is restricted to five time intervals because the chronology was limited to the last 100 years.

DDT, Ag, and Hg fluxes to site RB92-3 were reconstructed using the 20-year by 15-cm model grid with a 33-cm surface interval. Concentrations above background (Venkatesan et al., 1999; Hornberger et al., 1999) were converted to mass per cm^2 with missing intervals assigned by linear interpolation. Profiles were truncated at the deepest interval with detectable concentration above background. Concentrations were summed over model grid intervals and multiplied by the inverted matrix **F** to yield J. The reconstructed flux of DDT (Table 4) was greatest for the period of 1952–1971, with about 20% of the total DDT input occurring in the last 20 years. Because DDT usage was banned in 1972, the ongoing input may reflect the lag time in transport from the drainage basin and/or redistribution and transport within the estuary. Silver input also was greatest 20 to 40 years ago with a subsequent decrease of about 70%. Although 70% of the Ag input occurred within the last 40 years, a large input between 60 and

Table 4
Deconvolution model reconstructed contaminant fluxes to Richardson Bay site RB92-3

Years before 1992	Calendar years	Total DDT flux (ng/cm^2)	Ag flux ($\mu g/cm^2$)	Hg flux ($\mu g/cm^2$)
0–20	1972–1992	140	3.0	2.6
21–40	1952–1971	410	9.7	5.9
41–60	1932–1951	90	1.0	4.0
61–80	1912–1931	0	4.0	3.0
81–100	1892–1911	0	0	0

Fluxes are calculated total input to site RB92-3 during each 20-year time interval.

80 years ago was also calculated. Hg input was greatest 20 to 40 years ago, then decreased by a factor of two.

4.9. Apparent sediment chronology at San Pablo Bay

The radionuclide profiles indicate that the upper 120 cm of sediment column at SP90-8 was deposited within the last 30 to 40 years. An average sedimentation rate of 4 cm/year was calculated from the ^{137}Cs and ^{239,240}Pu maxima and dates were assigned to the upper 100 cm assuming negligible mixing or compaction. These assigned dates assume a constant and continuous sedimentation rate. No attempt was made to correct the dates shown in Fig. 7 for the thickness of sand layers and/or episodic deposition events.

The fallout radioisotopes were absent below 122 cm. Dates of 1958 and 1960 were calculated for the 122-cm horizon using the sedimentation rates from the ^{137}Cs and ^{239,240}Pu peaks, respectively. The maximum depth of ^{137}Cs and ^{239,240}Pu penetration should have been at 148 and 156 cm based on these rates, which is significantly deeper than measured maximum depth of penetration. The absence of measurable excess ^{210}Pb below 120 cm indicates that these sediments are at least 60 years old based on the excess ^{210}Pb detection limit. No additional constraint on sediment ages can be made from the radioisotope data.

Jaffe et al. (1998) estimated rates of sedimentation and erosion for San Pablo Bay using five detailed historical bathymetric surveys. Bathymetry data were corrected for tidal stage and averaged over 150 m^2 encompassing the location of site SP90-8, which is known to about 100 m. Changes in bathymetry at this site indicate that 220 cm of sediment were deposited between 1856 and 1897 and 20 cm between 1897 and 1921. Subsequently, net erosion of 70 cm occurred between 1921 and 1951, followed by net accumulation of 100 cm between 1951 and 1983. Assuming sediment accumulated at the 1951–1983 rate (3.1 cm/year) until 1990, about 22 cm more sediment accumulated for a total of 122 cm since 1951. A 63-year gap in the sedimentary record below 122 cm is suggested encompassing the period between 1888 and 1951. This assumes the 70-cm of erosion removed all 20-cm of sediment deposited between 1897 and 1922 and 50 cm deposited at the inferred 1856–1897 rate.

The average sedimentation rate from ^{137}Cs and ^{239,240}Pu is in reasonable agreement with the rate since 1951 estimated from bathymetry. The 60-year hiatus in the sedimentary record before this period is consistent with the common maximum depth of penetration of excess ^{210}Pb, ^{137}Cs and ^{239,240}Pu. The presence of sand layers throughout the sediment column, the inferred large-scale erosion, and the high sedimentation rates are indicative of a highly dynamic, non steady-state sedimentary environment at this site.

If the inferred age of over 100 years for sediment below 120 cm is correct, deeper sediments should contain material resulting from hydraulic gold mining between 1852 and 1884. This change in sediment source might explain the higher average ^{226}Ra activity below 120 cm. However, the ^{226}Ra activity of hydraulic mining debris has not been determined. Elevated Hg also was observed below this depth and was presumed to be related to gold mining during the last half of the 1800's (Hornberger et al., 1999).

5. Summary

At a site in Richardson Bay a sediment accumulation rate of 0.825 g/cm^2/year, surface mixing coefficient of 71 cm^2/year, and mixed depth of 33 cm were determined from the best fit simulation of the ^{210}Pb profile. A chronology for the date of first appearance of particle bound contaminants and for the date of maximum input over the last 100 years was developed from these best fit sediment accumulation and mixing rates. The rapid and deep sediment reworking of the upper 33 cm of the sediment column by biological and/or physical processes causes rapid dilution of sediment-bound contaminants upon deposition. The extensive mixing also results in the persistence of contaminants within the surface sediments for many years after deposition. It is estimated that about 50% of a contaminant deposited 35 years ago would remain in the mixed zone. Contaminant fluxes can be reconstructed from sediment profiles but are limited to 20-year time intervals because of extensive mixing.

In contrast, much lower sediment mixing relative to accumulation was evident at the San Pablo Bay site. Overall sedimentation rates on the order of 4 cm/year were estimated over the last 40 years from

^{210}Pb, ^{137}Cs and ^{239,240}Pu profiles. A hiatus in the sedimentary record prior to this period of about 60 years inferred from historic bathymetric records is consistent with the common maximum depth of penetration of all three radiotracers. The very high sedimentation rates and the apparent hiatus indicate that steady state sedimentation is unlikely at this site.

Acknowledgements

This work was funded in part by a cooperative agreement between the U.S. Geological Survey and the National Oceanographic and Atmospheric Administration under grant #1434-93-A-106. Fruitful discussions through all stages of this study and review of manuscript by S. Luoma are gratefully acknowledged. R. Rosenbauer and P. van Metre of the USGS provided helpful reviews of the manuscript, as did two anonymous reviewers.

References

Aller, R.C., DeMaster, D.J., 1984. Estimates of particle flux and reworking at the deep-sea floor using ^{234}Th/^{238}U disequilibrium. Earth Planet. Sci. Lett. 29, 308–318.

Aller, R.C., Benninger, L.K., Cochran, J.K., 1980. Tracking particle associated processes in nearshore environments by use of ^{234}Th/^{238}U disequilibrium. Earth Planet. Sci. Lett. 47, 161–175.

Aller, R.C., Cochran, J.K., 1976. ^{234}Th/^{238}U disequilibrium in nearshore sediment: particle reworking and diagenetic timescales. Earth Planet. Sci. Lett. 29, 37–50.

Appleby, P.G., Oldfield, F., 1992. Application of ^{210}Pb to sedimentation studies. In: Ivanovich, M., Harmon. R.S. (Eds.), Uranium-series Disequilibrium: Application to Earth, Marine, and Environmental Sciences, 2nd edn., Chap. 21. Clarendon Press, Oxford, pp. 731–778.

Baskaran, M., Naidu, A.S., 1995. ^{210}Pb-derived chronology and the fluxes of ^{210}Pb and ^{137}Cs isotopes into continental shelf sediments, East Chukchi Sea, Alaskan Arctic. Geochim. Cosmochim. Acta 59, 4435–4448.

Bopp, R.F., Simpson, H.J., Chillrud, S.N., Robinson, D.W., 1993. Sediment-derived chronologies of persistent contaminants in Jamaica Bay, New York. Estuaries 16, 608–616.

Callender, E., Robbins, J.A., 1994. Transport and accumulation of radionuclides and stable elements in a Missouri River reservoir. Water Resourc. Res. 29, 1787–1804.

Christensen, E.R., Bhunia, P.B., 1986. Modeling radiotracers in sediments: comparison with observations in Lakes Huron and Michigan. J. Geophys. Res. 91, 8559–8571.

Christensen, E.R., Goetz, R.H., 1987. Historical fluxes of particle-bound pollutants from deconvoluted sedimentary records. Environ. Sci. Technol. 21, 1088–1096.

Crusius, J., Anderson, R.F., 1991. Core compression and surficial sediment loss of lake sediments of high porosity caused by gravity coring. Limnol. Oceanogr. 36, 1021–1031.

Crusius, J., Anderson, R.F., 1995. Evaluating the mobility of ^{137}Cs, ^{239,240}Pu and ^{210}Pb from their distributions in laminated lake sediments. J. Paleolim. 13, 119–141.

Cutshall, N.H., Larsen, I.L., Olsen, C.R., 1983. Direct analysis of ^{210}Pb ins sediment samples: self-absorption corrections. Nucl. Inst. Meth. 306, 309–312.

Eisenreich, S.J., Capel, P.D., Robbins, J.A., Bourbonniere, R., 1989. Accumulation and diagenesis of chlorinated hydrocarbons in lacustrine sediments. Environ. Sci. Technol. 23, 1116–1126.

Flynn, W.W., 1968. The determination of low levels of polonium-210 in environmental materials. Anal. Chim. Acta 43, 221–227.

Friedlander, G., Kennedy, J.W., Miller, J.M., 1981. Nuclear and Radiochemistry. Wiley, New York. 585 pp.

Fuller, C.C., 1982. The use of ^{210}Pb, ^{234}Th, and ^{137}Cs as tracers of sedimentary processes in San Francisco Bay, California. Master's thesis, University of Southern California, 215 pp.

Fuller, C.C., Hammond, D.E., 1983. The fallout rate of ^{210}Pb on the western coast of the United States. Geophys. Res. Lett. 10, 1164–1167.

Goldberg, E.D., Koide, M., 1962. Geochronological studies of deep sea sediments by the ionium/thorium method. Geochim. Cosmochim. Acta 26, 417–450.

Guinasso, N.L., Schink, D.R., 1975. Quantitative estimates of biological mixing rates in abyssal sediments. J. Geophys. Res. 80, 3032–3043.

Health and Safety Laboratory, 1976. Final tabulation of monthly ^{90}Sr fallout data, 1954–1976. Health and Safety Lab. Environ. Quart., No. 329. U.S. Energy Research and Development Admin., NY, 884 pp.

Hill, B.R., Fuller, C.C., DeCarlo, E.H., 1997. Fluvial transport of atmospherically derived quartz and North Halawa Valley Oahu ^{137}Cs. Geomorphology 20, 67.

Hornberger, M.I., Luoma, S.N., van Geen, A., Fuller, C., Anima, R., 1999. Historical trends of metals in sediments of San Francisco Bay, California. Mar. Chem. 64, 39–55, (this issue).

Huh, C.-A., Kadko, D.C., 1992. Marine sediments and sedimentation processes. In: Ivanovich, M., Harmon. R.S. (Eds.), Uranium-series Disequilibrium: Application to Earth, Marine, and Environmental Sciences, 2nd edn., Chap. 13. Clarendon Press, Oxford, pp. 460–486.

Jaffe, B.E., Smith, R.E., Zink, L., 1998. Sedimentation and Bathymetry Changes in San Pablo Bay: 1856–1983. U.S. Geological Survey Open-File Report 98–759.

Kressin, I.K., 1977. Electrodeposition of plutonium and americium for high resolution alpha spectrometry. Anal. Chem. 49, 842–846.

Krom, M.D., Kaufman, A., Hornung, H., 1994. Industrial mercury in combination with natural ^{210}Pb as time-dependent tracers of sedimentation and mercury removal from Haifa Bay, Israel. Estuar. Coast. Shelf Sci. 38, 625–642.

McKee, B.A., Nittrouer, C.A., DeMaster, D.J., 1984. The use of $^{234}Th/^{238}U$ disequilibrium to examine the fate of particle reactive species on the Yangtze continental shelf. Earth Planet. Sci. Lett. 68, 431–442.

Olsen, C.R., Simpson, H.J., Peng, T.-H., Bopp, R.F., Trier, R.M., 1981. Sediment mixing and accumulation rate effects on radionuclide depth profiles in Hudson estuary sediments. J. Geophys. Res. 86, 11020–11028.

Olsen, C.R., Larsen, I.L., Mulholland, P.J., von Damm, K.L., Grebmeier, J.M., Schaffner, L.C., Diaz, R.J., Nichols, M.M., 1993. The concept of an equilibrium surface applied to particle sources and contaminant distributions in estuarine sediments. Estuaries 16, 683–696.

Peng, T.-H., Broecker, W.S., Berger, W.H., 1979. Rates of benthic mixing in deep-sea sediments determined by radiotracers. Quat. Res. 11, 141–149.

Pereira, W.E., Hostettler, F.D., Luoma, S.N., van Geen, A., Fuller, C.C., Anima, R., 1999. Sedimentary record of anthropogenic and biogenic polycyclic aromatic hydrocarbons in San Francisco Bay, California. Mar. Chem. 64, 99–113, (this issue).

Ravichandran, M., Baskaran, M., Santschi, P.H., Bianchi, T.S., 1995a. History of trace-metal pollution in Sabine-Neches estuary, Beaumont, Texas. Environ. Sci. Technol. 29, 1495–1503.

Ravichandran, M., Baskaran, M., Santschi, P.H., Bianchi, T.S., 1995b. Geochronology of sediments in the Sabine-Neches estuary, U.S.A. Chem. Geol. 125, 291–306.

Robbins, J.H., 1987. A model for particle-selective transport of tracers in sediments with conveyor belt deposit feeders. J. Geophys. Res. 91, 8542–8558.

Robbins, J.H., Edgington, D.N., 1976. Determination of recent sedimentation rates in Lake Michigan using ^{210}Pb and ^{137}Cs. Geochim. Cosmochim. Acta 39, 285–304.

Santschi, P.H., Li, Y.-H., Bell, J.J., Trier, R.M., Kawtaluk, K., 1980. Pu in the coastal marine environment. Earth Planet. Sci. Lett. 51, 248–265.

Santschi, P.H., Nixon, S., Pilson, M., Hunt, C., 1984. Accumulation of sediments, trace metals (Pb, Cu) and total hydrocarbons in Narragansett Bay, Rhode Island. Estuar. Coast. Shelf Sci. 19, 427–449.

Schwartz, M., 1998. Water Quality of San Francisco Bay, [http://sfbay.wr.usgs.gov/access/wqdata/], March 1998.

Simpson, H.J., Trier, R.M., Olsen, C.R., Hammond, D.E., Ege, A., Miller, L.G., Melack, J., 1980. Fallout plutonium in an alkaline, saline lake. Science 207, 1071–1073.

Smith, J.T., Comans, R.N.J., 1996. Modeling the diffusive transport and remobilization of ^{137}Cs in sediments: the effects of sorption kinetics and reversibility. Geochim. Cosmochim. Acta 60, 995–1004.

Turekian, K.K., Cochran, J.K., 1978. Determination of marine geochronologies using natural radionuclides. In: Riley, J.P., Chester, R. (Eds.), Chemical Oceanography, Vol. 7. Academic Press, New York, pp. 313–360.

Valette-Silver, N.J., 1993. The use of sediment cores to reconstruct historical trends in contamination in estuarine and coastal sediments. Estuaries 16, 577–588.

van Geen, A., Valette-Silver, N.J., Luoma, S.N., Fuller, C.C., Baskaran, M., Tera, F., Klein, J., 1999. Constraints on sedimentation history of San Francisco Bay from ^{14}C and ^{10}Be. Mar. Chem. 64, 29–38, (this issue).

van Metre, P.C., Callender, E., Fuller, C.C., 1997. Historical trends in organochlorine compounds in river basins identified using sediment cores from reservoirs. Environ. Sci. Technol. 31, 2339–2344.

Venkatesan, M.I., de Leon, R.P., van Geen, A., Luoma, S.N., 1999. Chlorinated hydrocarbon pesticides and polychlorinated biphenyls in sediment cores from San Francisco Bay. Mar. Chem. 64, 85–97, (this issue).

Wong, C.S., Sanders, G., Engstrom, D.R., Long, D.T., Swackhamer, D.L., Eisenreich, S.J., 1995. Accumulation, inventory, and diagenesis of chlorinated hydrocarbons in Lake Ontario sediments. Environ. Sci. Technol. 29, 2661–2672.